Continuous measurement of air-water gas exchange by underwater eddy covariance

Peter Berg, Michael. L. Pace

Department of Environmental Sciences, University of Virginia, Charlottesville, Virginia, USA

Correspondence to: Peter Berg (pb8n@virginia.edu)

10   **Abstract.** Exchange of gases, such as O_2, CO_2, and CH_4, over the air-water interface is an important component in aquatic ecosystem studies, but exchange rates are typically measured or estimated with substantial uncertainties. This diminishes the precision of common ecosystem assessments associated with gas exchanges such as primary production, respiration, and greenhouse gas emission. Here, we used the aquatic eddy covariance technique – originally developed for benthic

15   O_2 flux measurements – right below the air-water interface (~4 cm) to determine gas exchange rates and coefficients. Using an Acoustic Doppler Velocimeter and a fast-responding dual O_2-temperature sensor mounted on a floating platform the 3D water velocity, O_2 concentration, and temperature were measured at high-speed (64 Hz). By combining these data, concurrent vertical fluxes of O_2 and heat across the air-water interface were derived, and from the former, gas

20   exchange coefficients. Proof-of-concept deployments at different river sites gave standard gas exchange coefficients (k_{600}) in the range of published values. A 40 h long deployment revealed a distinct diurnal pattern in air-water exchange of O_2 that was controlled largely by physical processes (e.g., diurnal variations in air temperature and associated air-water heat fluxes) and not by biological activity (primary production and respiration). This physical control of gas exchange

25   can be prevalent in lotic systems and adds uncertainty to assessments of biological activity that are based on measured water column O_2 concentration changes. For example, in the 40 h

deployment, there was close-to constant river flow and insignificant winds – two main drivers of lotic gas exchange – but we found gas exchange coefficients that varied by several fold. This was presumably caused by the formation and erosion of vertical temperature-density gradients in the surface water driven by the heat flux into or out of the river that affected the turbulent mixing. This effect is unaccounted for in widely used empirical correlations for gas exchange coefficients and is another source of uncertainty in gas exchange estimates. The aquatic eddy covariance technique allows studies of air-water gas exchange processes and their controls at an unparalleled level of detail. A finding related to the new approach is that heat fluxes at the air-water interface can, contrary to those typically found in the benthic environment, be substantial and require correction of O_2 sensor readings using high-speed parallel temperature measurements. Fast-responding O_2 sensors are inherently sensitive to temperature changes, and if this correction is omitted, temperature fluctuations associated with the turbulent heat flux will mistakenly be recorded as O_2 fluctuations and bias the O_2 eddy flux calculation.

1 Introduction

1.1 Background

Exchange rates of gases over the air-water interface in rivers, streams, reservoirs, lakes, and estuaries are key parameters for estimating a number of important ecosystem variables (Cole et al. 2010). Gas exchange rates are used to estimate metabolism of aquatic systems (Hanson et al. 2004; Van de Bogert et al. 2007; Van de Bogert et al. 2012), emission of greenhouse gases like CO_2 and CH_4 to the atmosphere (Cole et al. 2010), and the role of inland and near-shore waters in regional (Billett and Moore 2008) and global (Cole et al. 2007; Bastviken et al. 2011) carbon cycling. As a result, over several decades a tremendous effort among aquatic scientists has focused on understanding and quantifying gas exchange processes at the air-water interface and their controls under naturally occurring field conditions (Whitman 1923; Butman and Raymond 2011; Raymond et al. 2013).

55   Multiple state variables and complex physical processes on both sides of the air-water interface
control gas exchange (Macintyre et al. 1995; MacIntyre et al. 2010). Despite this complexity, the
widely used expression for gas exchange rates was formulated based on a conceptually simple
model assuming that gas is transported by molecular diffusion across intact boundary layers, or
thin films, found on each side of the interface (Whitman 1923; Liss and Slater 1974):

60

$$J_{air-water} = k(C_{water} - C_{air}) \tag{1}$$

where $J_{air-water}$ is the exchange rate, or vertical flux, of the gas (positive upward), C_{water} is the gas
bulk concentration below the film on the water-side, C_{air} is the concentration above the film on the
65   air-side, and k is the gas exchange coefficient, often also referred to as the 'gas transfer velocity' or
'piston velocity'. For most gases, C_{water} and C_{air} are straight forward to measure with modern
sensors (Koopmans and Berg 2015; Fritzsche et al. 2017), or calculate from known functions, but
the complexity of gas exchange and its many controlling variables is contained in k (Macintyre et
al. 1995; McKenna and McGillis 2004; Cole et al. 2010).

70

For sparingly soluble gases such as O_2, CO_2, and CH_4, the ratio between the molecular diffusivity in
air and water is on the order of 10^4. Consequently, the resistance to gas diffusion is associated
with the film on the water-side, even if a substantially thicker film is found on the air-side of the
air-water interface. This means that in the case of O_2, C_{air} is simply the saturation concentration of
75   O_2 in water, which is a well-described function of the water temperature and salinity (Garcia and
Gordon 1992) and the atmospheric pressure.

Turbulence, or turbulent-like motions, that affects or controls the thickness of the film on the
water side, and thus the diffusive resistance to gas transport, can be driven by conditions both
80   below and above the air-water interface. In shallow streams and rivers, this turbulence is
typically generated by the water flow over an uneven or rough bottom. Substantial heat loss from
the water can similarly result in density driven water motion that erodes the film (Bannerjee and

MacIntyre 2004). On the contrary, in reservoirs, lakes, and estuaries, the turbulence on the water side of the interface is typically generated by wind, which makes wind speed the dominant controlling variable for k for such systems (Marino and Howarth 1993). Despite the fact that typical conditions such as rough weather, surface waves, and rain can rupture the film on the water side, the simple expression for gas exchange (Eq. 1) is still applied with k values that are adjusted accordingly (Watson et al. 1991). Keeping these multivariable, highly dynamic, and complex controls in mind, it is evident that determination of representative k values for specific sites is a challenging task.

1.2 Formulation of problem

A number of approaches have been used to study and determine values for k. For smaller rivers and streams they include targeted parallel up-and across-stream additions of volatile tracers (e.g. propane) and hydrologic tracers (e.g. dissolved chloride), where the latter is added to correct for dilution of propane due to hyporheic mixing (Genereux and Hemond 1992; Koopmans and Berg 2015). A common approach for smaller reservoirs and lakes relies on additions of inert tracers, e.g. SF_6 (Wanninkhof 1985; Cole et al. 2010), whereas floating chambers are often deployed in larger rivers, reservoirs, lakes, and estuaries (Marino and Howarth 1993). In a limited number of studies of large reservoirs and lakes, tower-mounted atmospheric eddy covariance systems have been used to measure air-water exchange, and from that, k values were derived (Anderson et al. 1999; Jonsson et al. 2008; Mammarella et al. 2015). Partly motivated by the substantial and often methodologically challenging effort required to measure k at specific sites with any of these approaches, many studies have simply relied on general empirical correlations for k produced by fitting k values measured for other similar aquatic systems (Raymond and Cole 2001; Borges et al. 2004; Cole et al. 2010). With the exception of atmospheric eddy covariance measurements, none of these approaches represent a direct way of determining k values because they rely on assumptions that often are difficult to assess, or simply not fulfilled. As a result, gas exchange is viewed among aquatic scientists as the primary source of uncertainty in many standard estimates

for aquatic systems such as gross primary production, respiration, and net ecosystem metabolism (Wanninkhof et al. 1990; Raymond and Cole 2001; Raymond et al. 2012).

1.3 Scope of work

The aquatic eddy covariance technique for O_2 flux measurements under undisturbed in situ conditions was originally developed for the benthic environment (Berg et al. 2003). The approach has several significant advantages over other flux methods, including its non-invasive nature (Lorrai et al. 2010), high temporal resolution (Rheuban & Berg 2013), and its ability to integrate over a large benthic surface (Berg et al. 2007). As a result, it has been used to measure whole-system fluxes for substrates such as river bottoms (Lorke et al. 2012; Berg et al. 2013), seagrass meadows (Hume et al. 2011; Rheuban et al. 2014), and coral reefs (Long et al. 2013; Rovelli et al. 2015).

Here, we applied the aquatic eddy covariance technique 'upside down' right below the air-water interface to measure O_2 fluxes. From them, we derived exchange coefficients for O_2, and then standard gas exchange coefficients (k_{600}). All measurements were done from a floating platform, and because we used a newly developed fast-responding dual O_2-temperature sensor (Berg et al. 2016), we were able to derive parallel fluxes of O_2 and thermal energy, or sensible heat. We conducted proof-of-concept tests that were up to 40 h long at three river sites.

2 Methods

2.1 Floating measurements platform

All measurements were made from a 1.2 × 0.9 m floating platform with a catamaran-shaped hull (Fig. 1) that was kept at a fixed position at the river sites by two upstream anchors. The modular design and the catamaran-shaped hull allow the platform to be collapsed for storage and easy shipment in a standard sturdy Polymer case (Pelican Products, USA).

The 3D velocity field was measured with an Acoustic Doppler Velocimeter (ADV) with a cabled sensor head (cabled Vector, Nortek AS, Norway). This type of ADV allowed the sensor head to be positioned facing upwards (Fig. 1) while recording the velocity field right below the air-water interface, typically ~4 cm. This distance was determined from standard ADV output. Data were collected continuously at a rate of 64 Hz and represent water velocity values averaged over the ADV's cylindrical measuring volume (h ~1.4 cm, Ø ~1.4 cm) located 15.7 cm above the sensor head (Fig. 1).

The O_2 concentration was measured with a new fast-responding dual O_2-temperature sensor (RINKO EC, JFE Advantech, Japan) developed specifically for eddy covariance measurements (Berg et al. 2016). This sensor allows for simultaneous fluxes of O_2 and heat to be derived. It also allows instantaneous temperature correction of the O_2 concentration. The sensor was designed to interface with our standard ADVs (Vectors, Nortek AS, Norway) through a single cable supplying power to the sensor and also transmitting its two outputs, one for O_2 and one for temperature, to the ADV's data logger to be recorded along with velocities to ensure perfect time alignment of all data. The O_2 measuring part of this new sensor is a small 6 mm diameter planar optode and concentrations are determined from fluorescence life-time measurements (Klimant et al. 1995; Holst et al. 1997; Holst et al. 1998). The tip of the sensor which contains both the temperature thermistor and the O_2 sensing foil, has a diameter of 8.0 mm which makes it far more robust than O_2 microsensors typically used for aquatic eddy covariance measurements. Yet because the sensor's tip is still only half the size of the ADV's measuring volume, it will not limit the eddy size that can be measured by the system. The sensor's response times ($t_{90\%}$) were measured to be 0.51 ± 0.01 s (SE, n = 7) for O_2 and 0.34 ± 0.01 s (SE, n = 9) for temperature (Berg et al. 2016). The same response time for O_2 was consistently found when the O_2 sensing foil was replaced (an easy user performed operation typically needed after ~10 days of continuous use). The edge of the sensor tip was positioned ~2.0 cm downstream of the edge of the ADV's measuring volume so that water passed through this volume before sweeping over the angled O_2 sensing tip (Fig. 1a). This setup ensured undisturbed measurements of the natural current flow. Power was supplied

from an external battery (Fig. 1a) with a capacity that allowed 64 Hz data to be collected continuously for at least 48 h. Because all instrument components were designed for underwater use they are not affected by rain or humid conditions.

170 Measurement of supporting environmental variables during each deployment allowed verification of recorded data and assisted in the interpretation of the derived eddy fluxes. These variables included mean O_2 concentration and temperature at the measuring depth recorded every 1 min with one or two stable independent dual O_2-temperature sensors (miniDOT, PME, USA, referred to as the independent sensor below). In most deployments photosynthetically
175 active radiation (PAR) was recorded at the measuring depth every 5 min using an independent submersible PAR sensor (Odyssey, Dataflow Systems, New Zealand). For one deployment, light data were taken from nearby meteorological weather stations.

2.2 Field tests

180 The new approach for determining air-water gas exchange rates and associated exchange coefficients from underwater eddy covariance measurements was tested at three river sites, all in Virginia (US), one in the Hardware River, one in the Mechums River, and one in Moormans River. All sites had a fairly linear run with a water depth between ~0.3 and ~1 m and smooth and quietly flowing water without standing riffles or waves. As a result of this, the two-point
185 anchoring system, and the current's constant pull on the hull, the platform was stationary during measurements. Typical surface flow velocities ranged from 6 to 30 cm s^{-1}. The ADV and the fast-responding O_2-temperature sensor were adjusted to record data ~4 cm below the air-water interface. Four deployments lasting up to 40 h were initiated on November 22, 2015 and September 14, 2016 in the Hardware River and on December 21, 2016 and January 18, 2017 in
190 the Moormans River. Using a level and by placing dive weights on the platform (Fig. 1b) care was taken to ensure that the platform was horizontal within the tolerance of the level to minimize post-processing rotations of the velocity field to correct for sensor tilt.

2.3 Calculations of eddy fluxes

195 Fluxes of O_2 were extracted from the raw eddy covariance data following the multi-step process briefly described below.

Using the two simultaneously measured outputs from the fast-responding dual O_2-temperature sensor, one for O_2 and one for temperature, the O_2 concentration was calculated from the
200 calibration equation provided by the manufacture. Because this equation contains both outputs, this calculation includes instantaneous temperature correction of the O_2 concentration evaluated in detail below. If needed, the O_2 concentration was calibrated against the independent sensor data. All 64 Hz data were then reduced to 8 Hz data, which reduces noise while providing sufficient resolution to contain the full frequency spectrum carrying the detectable flux signal
205 (Berg et al. 2009). This assumption was validated by comparing fluxes calculated from both 8 and 64 Hz data for a subset of the data.

O_2 fluxes, one for each 15-min data segment, were extracted from the 8 Hz data using the software package EddyFlux version 3.1 (P. Berg unpubl.). If needed, this software rotates the flow velocity
210 field for each data segment to correct for any sensor tilt (Lee et al. 2004; Lorrai et al. 2010; Lorke et al. 2013) bringing the transverse and vertical mean velocities to zero. The vertical eddy flux was then calculated as (defined positive upward):

$$J_{eddy} = \overline{w'C'} \qquad (2)$$

215

where the overbar symbolizes the averaging over the 15-min data segment, and w' and C' are the fluctuating vertical velocity and the fluctuating O_2 concentration, respectively. These fluctuating components are calculated as $w - \overline{w}$ and $C - \overline{C}$ where w and C are measured values (at 8 Hz), and $\overline{w}$ and $\overline{C}$ are mean values defined as least square linear fits to all w and C values within the 15-min

time segment, a procedure usually referred to as linear de-trending (Lee et al. 2004; Berg et al. 2009).

Due to the response time of the dual O_2-temperature sensor and its position downstream from the ADV's measuring volume, a time shift correction was applied. This was done by repeating the outlined flux calculation, while shifting the 8 Hz O_2 concentration data back in time, 1/8 s at a time, until the numerically largest flux was found.

Estimating the gas exchange coefficient requires the O_2 flux over the air-water interface to be known. However, the eddy flux, J_{eddy} (Eq. 2), is measured ~4 cm below the interface. By using the linear fit to the measured O_2 concentrations in each 15-min data segment, defined as $\bar{C}$ above, J_{eddy} is corrected for storage of O_2 in the ~4 cm column of water to give the flux at the air-water interface:

$$J_{eddy,\,air-water} = J_{eddy} - \int_0^h \frac{d\bar{C}}{dt} dz \qquad (3)$$

where h is the ~4 cm tall water column, and the integral represents the change in time of O_2 stored in this column. For further details on this flux extraction protocol included in EddyFlux version 3.1, see Lorrai et al. (2010), Hume et al. (2011), and Rheuban et al. (2014). For presentation, the 15-min fluxes were lumped in groups of four to give hourly values.

To examine the eddy frequencies that carried the flux signal, cumulative co-spectra of the O_2 concentration and the vertical velocity were calculated for representative periods in each deployment using the software package Spectra version 1.2 (P. Berg unpubl.). This software essentially performs the identical flux calculation in the frequency domain after fast Fourier transforming the de-trended data as EddyFlux does in the time domain. Both software packages rely on the same methods for de-trending and time shifting data.

Heat fluxes and associated co-spectra were extracted from the raw eddy covariance data following the same multi-step process.

250

2.4 Calculations of gas exchange coefficients

The saturation concentration of O_2 (C_{air} in Eq. 1) was calculated from Garcia and Gordon (1992) as a function of salinity (here 0 ‰) and surface water temperature measured with the fast-responding dual O_2-temperature sensor ~4 cm below the air-water interface and then corrected

255 for actual atmospheric pressure using Henry's law (average sea-level pressure of 1013.25 mbar corrected for elevation). The water column O_2 bulk concentration (C_{water} in Eq. 1) was measured with the same sensor. By substituting $J_{air-water}$ (Eq. 1) with the 15-min values for $J_{eddy,\ air-water}$ (Eq. 3), a gas exchange coefficient for O_2 was calculated from Eq. 1 and converted to the standard exchange coefficient, k_{600}, for CO_2 at 20 °C (Cole et al. 2010). For presentation, the 15-min k_{600}

260 values were lumped in groups of four to give hourly values.

3   Results

All four deployments resulted in high-quality time series of the velocity field, the O_2 concentration, and the temperature ~4 cm below the air-water interface, and derived from those,

265 air-water fluxes of O_2 and heat, and gas exchange coefficients. These data and their interpretation are presented below.

3.1 Data example

For a 40 h long deployment initiated on January 18, 2017 in the Moormans River, the 15-min

270 mean current velocity (Fig. 2a) was relatively constant, averaging 20.5 cm s^{-1}. The O_2 concentration measured with the fast-responding dual O_2-temperature sensor (Fig. 2b) agreed closely with the concentration recorded with the independent sensor and showed a distinct diurnal pattern. During most of the first night of the deployment, the O_2 concentration increased linearly (h 19 to h 32), whereas a smaller and non-linear increase that tapered off was measured

during the second night (h 45 to h 56). A diurnal pattern was also seen in the calculated O_2 saturation concentration (Fig. 2b) reflecting variation in water temperature. The cumulative O_2 flux (Fig. 2c), with each data segment covering a 15-min time interval, had clear linear trends indicating a strong eddy flux signal in the data. The hourly O_2 flux (Fig. 2d), representing means of four successive 15-min flux estimates, also exhibited a clear diurnal pattern with a nighttime average uptake by the river of 16.4 mmol m^{-2} d^{-1} for the first night, 9.1 mmol m^{-2} d^{-1} for the second night, and an average daytime release of 11.1 mmol m^{-2} d^{-1}. As observed for the O_2 concentration (Fig. 2b), the hourly O_2 flux differed during the two nighttime periods with a close-to constant flux during the first night and a flux that tapered off during the second night. The hourly standard gas exchange coefficient (k_{600}, Fig. 2e) derived from the 15-min O_2 flux and the O_2 concentration difference over the air-water interface (Fig. 2b) was almost constant over the first night of the deployment with an average of 3.9 m d^{-1}. After that, k_{600} diminished almost 3-fold to a value of 1.4 m d^{-1} during the daytime. During the second night, k_{600} tapered off markedly from a level found for the first night to almost 0.89 m d^{-1} during the last four h of the deployment. This pattern was unexpected given the almost constant mean current velocity and insignificant winds (Fig. 2a) and the similar O_2 concentration difference (Fig. 2b) for the two nighttime periods. The pattern suggests that gas exchange was controlled by at least one driver apart from the river current velocity or winds (see Discussion below).

The parallel results derived from the temperature data measured with the fast-responding dual O_2-temperature sensor agreed perfectly with the temperature recorded with the independent sensor (Fig. 3b) and had, as with the O_2 concentration, a distinct diurnal pattern. A close-to linear decrease occurred during the first night (h 18 to h 32) whereas a smaller and non-linear decrease that tapered off was recorded during the second night (h 45 to h 56). During the daytime the temperature increased. Unfortunately, we do not have reliable on-site measurements of the air temperature, but we infer that it, together with shortwave (sunlight during day) and longwave (nighttime) thermal radiation, controlled the recorded water temperature variations (Fig. 3b). The cumulative heat flux (Fig. 3c) had, as for O_2, clear linear trends indicating a strong flux signal

in the data. The hourly heat flux (Fig. 3d) also exhibited a clear diurnal pattern with a nighttime average release of heat of 60.6 W m^{-2} for the first night and 27.5 W m^{-2} for the second night. As was observed for the temperature (Fig. 3b), the hourly heat flux showed different trends for the two nights with a close-to constant flux during the first night and a flux that tapered off during the second night.

Ignoring differences in the sign, representative cumulative co-spectra for the O_2 and heat fluxes (Fig. 4) during the first night (Figs. 2, 3) were similar in the 0.1 to 1 Hz frequency band with all substantial flux contributions for both the O_2 and heat fluxes having frequencies lower than ~0.9 Hz.

Due to careful leveling of the platform prior to data collection (Fig. 1b), rotation of the velocity field to correct for sensor tilt was minimal with an average of only 1.3° from horizontal. This rotation had an insignificant effect on the flux calculation. The applied time shift averaged 1.3 and 1.2 s for the O_2 and heat flux calculations, respectively, whereas the average storage correction (Eq. 3) amounted to 11 % for the O_2 flux and 15 % for the heat flux.

3.2 Representative gas exchange coefficients

The three other test deployments were shorter than the one presented in Figs. 2 and 3 but results were of comparable quality. Average values for selected parameters covering periods of time with several successive 15-min time intervals from all four deployments are given in Table 1. These periods were identified by containing consecutive time intervals with consistent standard gas exchange coefficient values, k_{600}, that had little variation and appeared to represent a particular field condition. The longest period ($n = 51$) covers the first full night of the deployment shown in Fig. 2 (h 19 to h 32). Overall, the average current velocity varied from 8.3 to 28.4 cm s^{-1} while k_{600} ranged from 0.4 to 5.1 m d^{-1}, or more than a factor of 12.

330   There was no significant relationship ($R = 0.37$, $p = 0.22$) between river current velocity and k_{600}

values (Fig. 5) for all of the data in Table 1. Substantial variations in k_{600} values were found for

some individual deployments even though the current velocity did not change markedly. Most

prominently in the Moormans River deployment (Figs. 2, 3), where the k_{600} values varied more

than a factor of 5. As we discuss below, this suggest that, at least for some sites and under some

335   field conditions, other drivers of air-water gas exchange than river flow and winds are more

important.

3.3 Temperature effects on O_2 readings – a possible methodological bias

In the benthic environment the vertical turbulent heat flux is usually small relative to the O_2 flux

340   due to slowly and modestly varying mean temperatures in the bottom water. At the air-water

interface, however, the heat flux is typically larger due to substantial variations in air temperature

and short- and long-wave thermal radiation, and the associated turbulent heat fluctuations can

represent a challenge in O_2 flux measurements by eddy covariance.

345   All highly sensitive fast-responding O_2 sensors that can be used for aquatic eddy covariance

measurements are to the best of our knowledge inherently sensitive to temperature changes, and

thus give variable O_2 readings at the same molar O_2 concentration if the temperature varies.

Typical temperature coefficients (% change in O_2 concentration reading caused by a temperature

change of 1 °C) for Clark-type microelectrodes, still the most common sensor type used for

350   aquatic eddy covariance, have values of ~3 % (Gundersen et al. 1998). Lab measurements in

which the O_2 concentration was held constant but temperature varied showed that the fast-

responding dual O_2-temperature sensor used in this study has a temperature coefficient of 2.9 %

if temperature correction was omitted. This characteristic of fast-responding O_2 sensors implies

that rapid temperature fluctuations associated with a turbulent heat flux will mistakenly be

355   recorded as fluctuations in O_2 concentration and bias the eddy flux calculation unless an

instantaneous temperature correction of the O_2 signal is performed. In this study, this correction

was done using the fast-responding dual O_2-temperature sensor's temperature reading from

within a few mm of the O_2 sensing foil. Below, we exemplify the nature and magnitude of this potential bias using data measured during the first night (h 18 to h 32) of the deployment shown in Figs. 2 and 3.

The turbulent temperature fluctuations for a 3-min period shown in Fig. 6a are associated with a vertical heat flux of ~60 W m^{-2} (Fig. 3d) and amount to ± ~0.015 °C. Based on a temperature coefficient of ~3 %, this translates into fluctuations in O_2 concentration readings of ± ~0.2 μmol L^{-1} (Fig. 6a, right axis). Using such 'simulated' O_2 data, derived from the 8 Hz nighttime temperature data (Fig. 3, h 18 to h 32), representing solely temperature sensitivity effects and no true O_2 reading, produced an O_2 release, or flux bias, of 11.9 mmol m^{-2} d^{-1} (blue bar, Fig. 6b). Using the instantaneous temperature corrected O_2 data, as was done for all other calculations we present, gives an oppositely directed O_2 uptake of 16.9 mmol m^{-2} d^{-1} (red bar, Fig. 6b). Using the sensor's O_2 readings, but without the instantaneous temperature correction, gives a release of only 4.4 mmol m^{-2} d^{-1} (green bar, Fig. 6b).

The magnitude of this O_2 flux bias if temperature correction is omitted, scales with the heat flux and is proportional with the O_2 sensor's temperature coefficient and the actual O_2 concentration. Given the mm-close proximity of the temperature thermistor and the O_2 sensing foil and the relatively small difference between the fast-responding dual O_2-temperature sensor's response times (0.51 for O_2 and 0.34 s for temperature, Berg et al., 2016), we conclude that the effects of temperature sensitivity were removed from our O_2 flux calculations. This point is supported by the high-frequency end (~0.9 Hz) of the co-spectra for the O_2 and heat fluxes (Fig. 4).

4 Discussion

Deploying the aquatic eddy covariance technique right below the air-water interface provided a feasible way to determine gas exchange rates and coefficients. Relative to what is possible with traditional methods, this new approach gives gas exchange rates and coefficients with an improved precision and at a higher spatial and temporal resolution. For those reasons, the

approach has the potential to enhance our knowledge of the dynamics and controls of gas exchange and thus benefit aquatic ecosystem studies and pave the way for new lines of ecosystem research.

390   These points are exemplified in our longest test deployment that lasted 40 h (Figs. 2, 3) and resulted in aquatic eddy covariance data for both O_2 and temperature of a quality and internal consistency that fully match those published for many benthic environments (see review by Berg et al. (2017)). Specifically, the 8 Hz velocity, O_2, and temperature data (Figs. 2a, 2b, 3b) were recorded with low noise and the O_2 and temperature data perfectly matched measurements with

395   the stable independent sensor (Figs. 2b, 3b). Furthermore, the cumulative fluxes (Figs. 2c, 3c) had clear linear trends that indicate a strong and consistent flux signal in the data, and the times where the hourly O_2 flux changed direction (Fig. 2d, positive values represent a release), matched exactly the times when the driving O_2 concentration difference changed sign (Fig. 2b). Moreover, the cumulative co-spectra for the O_2 and heat fluxes (Fig. 4) have the shape typically seen for

400   shallow-water environments (Lorrai et al. 2010; Berg et al. 2013). The fact that all flux contributions for both the O_2 and heat fluxes had frequencies lower than ~0.9 Hz, combined with the fast-responding dual O_2-temperature sensor's response times ($t_{90\%}$) of 0.51 s for O_2 and 0.34 s for temperature (Berg et al. 2016), indicates that the entire flux signal over all frequencies was captured. Finally, for both O_2 and temperature there was a clear relationship between the flux

405   over the air-water interface (Figs. 2d, 3d) and the observed change in the water column (Figs. 2b, 3b). For O_2, for example, the ratio between the averaged fluxes for the two nights (Fig. 2d, h 21 to h 30 vs. h 45 to h 54) equals 2.0 which is close to the ratio of 2.2 between the changes in water column concentrations (Fig. 2b) for the same two periods.

410   Both the O_2 and temperature data (Figs. 2b, 2d, 3b, 3d) contained a clear diurnal signal overall. For O_2, however, this was not driven by biological processes, i.e. net primary O_2 production during daytime and respiration during nighttime, as this would have resulted in an increase in mean water column O_2 concentration during daytime and a decrease at nighttime. That the opposite

pattern was found indicates that physical processes related to thermal conditions were controlling the O_2 dynamics. Specifically, colder nighttime air temperatures and possibly also long-wave thermal radiation to the atmosphere were driving the substantial heat flux out of the river (Fig. 3d) which resulted in falling water temperatures (Fig. 3b). This, in turn, changed the O_2 saturation concentration (C_{air} in Eq. 1) and thus the driving concentration difference of O_2 exchange over the air-water interface (Fig. 2b). During the daytime, the reverse pattern was in place. This rather complex relationship, or linkage via physical processes, is the only mechanism that can explain the overall pattern found for this deployment (Figs. 2, 3). Considering that these measurements were done under conditions that did not include any uncommon or extreme weather conditions suggests that physical processes, and not biological processes, are often an important, or even the main, driver of O_2 dynamics in shallow-water rivers and streams. An unfortunate consequence of this dominance or control by physical conditions, which we believe is not yet fully recognized, is that it adds substantial uncertainty to the widely used approach of deriving metabolic estimates (e.g., gross primary production, respiration, net ecosystem metabolism) from time series of measured water column O_2 concentrations (Odum 1956; Hall et al. 2016).

The standard gas exchange coefficients (k_{600}) for all of our four deployments (distributed on three different river sites, all with smooth quietly flowing water without standing riffles or waves, Fig.1) did not show a significant relationship with river current velocity (Fig. 5, Table 1). This is in line with previously published results from across-site comparisons (Hall et al. 2016), but the substantial variation among k_{600} values for some individual deployments (in particular for the Moormans River deployment, Fig. 2d) despite only moderately varying river flow velocity and insignificant winds is surprising. For example, k_{600} varied from a close-to constant value of 3.9 m d^{-1} during the first night (Fig. 2e, h 19 to h 32), followed by an almost 3 times smaller daytime value of 1.4 m d^{-1} (h 33 to h 42), and then increased again at the onset of the second night before finally tapering off to a small value of 0.9 m d^{-1} (h 52 to h 56) at the end of the deployment. The co-variance of the heat exchange (Fig. 3d) suggests that turbulence, or turbulent-like motions (which

stimulates gas exchange) was generated by natural convective forces driven by the substantial heat-loss from the river during the nighttime (Fig. 3d). Conversely, during the daytime, when the heat flux was directed into the river (Fig. 3d), turbulent motions were presumably dampened by

445   vertical temperature stratifications in the surface water. Given the 'low-energy' smooth and quietly flowing water, we find this explanation for the varying k_{600} values (Fig. 2e) likely and note that this controlling factor has been described before (Bannerjee and MacIntyre 2004; MacIntyre et al. 2010). We also note that this observed complex pattern illustrates the difficulties that can be associated with determining accurate air-water gas exchange rates and coefficients without direct

450   site- and time-specific measurements.

An important methodological finding linked to the new approach is that O_2 sensor readings should, at least in some cases, be corrected for temperature sensitivity using concurrent high-speed temperature readings as was done here for all O_2 fluxes used to estimate air-water gas

455   exchange coefficients (Fig. 2, Table 1). In the benthic environment the vertical turbulent heat flux is usually small relative to the O_2 flux due to slowly and modestly varying mean temperatures in the bottom water. However, results presented here show that rapid temperature fluctuations associated with the substantial turbulent heat flux below the air-water interface can mistakenly be recorded as fluctuations in the O_2 concentration and bias the O_2 flux calculation significantly if

460   instantaneous temperature correction is omitted (Fig. 6). It is unclear how widespread this problem is – more studies are needed to determine that – but in the example included here, this bias alters the flux by more than a factor of 3 (Fig. 6). Our data were recorded during winter, and one could argue that the O_2 exchange would be much larger during summer due to extensive primary production and respiration which would reduce the relative magnitude of this bias (Fig.

465   6). But as the O_2 flux is indeed likely to be more pronounced during summer than during winter, so is the heat flux.

5 Summary and recommendations

Based on our proof-of-concept deployments, the aquatic eddy covariance technique applied right below the air-water interface should be particularly useful in detailed studies of gas exchange that evaluate its dynamics and controls. The approach can consequently help reduce the generally recognized problem of large uncertainties linked to gas exchange estimates in traditional aquatic ecosystem studies.

The floating platform we used here for measuring aquatic eddy covariance fluxes right below the air-water interface (Fig. 1) can easily be reproduced as it relies exclusively on standard materials and commercially available instrumentation, the latter designed with plug-and-play capabilities. Furthermore, standard software for eddy flux extractions developed for the benthic environment or for the atmospheric boundary layer can be used to estimate air-water fluxes.

We recommend that eddy covariance data are recorded close to the air-water interface (Fig. 1c) to minimize the effects of the O_2 storage in the water between the measuring point and the surface and because gradients of both O_2 and temperature can form in the upper water column. We also recommend that simultaneous high-speed temperature measurements are performed within a few mm of the O_2 concentration recordings to allow for instantaneous temperature correction of the O_2 signal (Fig. 6).

Finally, our results illustrate that the O_2 concentration difference driving the air-water gas exchange is often small (Fig. 2), here < 2 % of the absolute concentration. This emphasizes the importance of relying both on accurately calibrated sensors to measure the water bulk concentration (C_{water} in Eq. 1) and precise determinations of the saturation concentration (C_{air} in Eq. 1) that is corrected for temperature, salinity, and atmospheric pressure.

6 Future work

A further development of the new application of the aquatic eddy covariance technique presented here is to perform similar measurements from a moving platform in small lakes, reservoirs, and estuaries. In these environments, gas exchange and gas exchange coefficients are expected to vary spatially, for example from the lee to windward side of the aquatic system. By using a floating autonomously moving platform, we anticipate that such variations can be spatially mapped out and studied. We are currently performing the first tests along these lines.

7 Acknowledgements

This study was supported by grants from the National Science Foundation (ESC-1550822, OCE-1334848) and the University of Virginia. We thank Julie and John Baird, Nancy and Ed Mcmurdo, Martha Hodgkins, and Brian Richter who allowed us to work on their beautiful properties in the Hardware River, the Mechums River, and the Moormans River. Finally, we thank Rachel E. Michaels for editorial assistance on the manuscript.

8 References

Anderson, D. E., R. G. Striegl, D. I. Stannard, C. M. Michmerhuizen, T. A. McConnaughey, and J. W. LaBaugh. 1999. Estimating lake-atmosphere CO2 exchange. Limnol. Oceanogr. **44:** 988-1001.

Bannerjee, S., and S. MacIntyre. 2004. The air–water interface: turbulence and scalar interchange. Advances in coastal and ocean engineering **9:** 181-237.

Bastviken, D., L. J. Tranvik, J. A. Downing, P. M. Crill, and A. Enrich-Prast. 2011. Freshwater Methane Emissions Offset the Continental Carbon Sink. Science **331:** 50-50.

Berg, P., M. L. Delgard, R. N. Glud, M. Huettel, C. E. Reimers, and M. L. Pace. 2017. Non-invasive Flux Measurements at the Benthic Interface: the Aquatic Eddy Covariance Technique. Limnol. Oceanogr.: e-Lectures **doi: 10.1002/loe2.10005**.

Berg, P., D. Koopmans, M. Huettel, H. Li, K. Mori, and A. Wüest. 2016. A new robust dual oxygen-temperature sensor for aquatic eddy covariance measurements. Limnol. Oceanogr.: Methods **14:** 151–167.

Berg, P., M. H. Long, M. Huettel, J. E. Rheuban, K. J. McGlathery, R. W. Howarth, K. H. Foreman, A. E. Giblin, and R. Marino. 2013. Eddy correlation measurements of oxygen fluxes in permeable sediments exposed to varying current flow and light. Limnol. Oceanogr. **58:** 1329–1343.

Berg, P., H. Roy, F. Janssen, V. Meyer, B. B. Jorgensen, M. Huettel, and D. de Beer. 2003. Oxygen uptake by aquatic sediments measured with a novel non-invasive eddy-correlation technique. Marine Ecology Progress Series **261:** 75-83.

Billett, M., and T. Moore. 2008. Supersaturation and evasion of CO2 and CH4 in surface waters at Mer Bleue peatland, Canada. Hydrological Processes **22:** 2044-2054.

Borges, A. V., B. Delille, L. S. Schiettecatte, F. Gazeau, G. Abril, and M. Frankignoulle. 2004. Gas transfer velocities of CO2 in three European estuaries (Randers Fjord, Scheldt, and Thames). Limnol. Oceanogr. **49:** 1630-1641.

Butman, D., and P. A. Raymond. 2011. Significant efflux of carbon dioxide from streams and rivers in the United States. Nature Geoscience **4:** 839-842.

Cole, J. J., D. L. Bade, D. Bastviken, M. L. Pace, and M. Van de Bogert. 2010. Multiple approaches to estimating air-water gas exchange in small lakes. Limnology And Oceanography-Methods **8:** 285-293.

Cole, J. J., Y. T. Prairie, N. F. Caraco, W. H. McDowell, L. J. Tranvik, R. G. Striegl, C. M. Duarte, P. Kortelainen, J. A. Downing, J. J. Middelburg, and J. Melack. 2007. Plumbing the global carbon cycle: Integrating inland waters into the terrestrial carbon budget. Ecosystems **10:** 171-184.

Fritzsche, E., P. Gruber, S. Schutting, J. P. Fischer, M. Strobl, J. D. Müller, S. M. Borisov, and I. Klimant. 2017. Highly sensitive poisoning-resistant optical carbon dioxide sensors for environmental monitoring. Analytical Methods **9:** 55-65.

Garcia, H. E., and L. I. Gordon. 1992. Oxygen solubility in seawater: Better fitting equations. Limnol. Oceanogr. **37:** 1307-1312.

Genereux, D. P., and H. F. Hemond. 1992. Determination of gas exchange rate constants for a small stream on Walker Branch Watershed, Tennessee. Water Resources Research **28:** 2365-2374.

Gundersen, J. K., N. B. Ramsing, and R. N. Glud. 1998. Predicting the signal of O-2 microsensors from physical dimensions, temperature, salinity, and O-2 concentration. Limnology & Oceanography **43:** 1932-1937.

555   Hall, R. O., J. L. Tank, M. A. Baker, E. J. Rosi-Marshall, and E. R. Hotchkiss. 2016. Metabolism, gas exchange, and carbon spiraling in rivers. Ecosystems **19:** 73-86.

Hanson, P. C., A. I. Pollard, D. L. Bade, K. Predick, S. R. Carpenter, and J. A. Foley. 2004. A model of carbon evasion and sedimentation in temperate lakes. Global Change Biology **10:** 1285-1298.

Holst, G., R. N. Glud, M. Kuhl, and I. Klimant. 1997. A Microoptode Array For Fine-Scale
560   Measurement of Oxygen Distribution. Sensors & Actuators B Chemical **38:** 122-129.

Holst, G., O. Kohls, I. Klimant, B. Konig, M. Kuhl, and T. Richter. 1998. A modular luminescence lifetime imaging system for mapping oxygen distribution in biological samples. Sensors and Actuators B-Chemical **51:** 163-170.

Hume, A. C., P. Berg, and K. J. McGlathery. 2011. Dissolved oxygen fluxes and ecosystem metabolism
565   in an eelgrass (Zostera marina) meadow measured with the eddy correlation technique. Limnol. Oceanogr. **56:** 86-96.

Jonsson, A., J. Åberg, A. Lindroth, and M. Jansson. 2008. Gas transfer rate and CO2 flux between an unproductive lake and the atmosphere in northern Sweden. Journal of Geophysical Research: Biogeosciences **113**.

570   Klimant, I., V. Meyer, and M. Kuehl. 1995. Fiber-optic oxygen microsensors, a new tool in aquatic biology. Limnol. Oceanogr. **40:** 1159-1165.

Koopmans, D. J., and P. Berg. 2015. Stream oxygen flux and metabolism determined with the open water and aquatic eddy covariance techniques. Limnol. Oceanogr. **60:** 1344-1355.

Liss, P., and P. Slater. 1974. Flux of gases across the air-sea interface. Nature **247:** 181-184.

575   Long, M. H., P. Berg, D. de Beer, and J. C. Zieman. 2013. In situ coral reef oxygen metabolism: An eddy correlation study. Plos One **8:** e58581. doi:58510.51371/journal.pone.0058581.

Lorke, A., D. F. McGinnis, A. Maeck, and H. Fischer. 2012. Effect of ship locking on sediment oxygen uptake in impounded rivers. Water Resources Research **48**.

Lorrai, C., D. F. McGinnis, P. Berg, A. Brand, and A. Wüest. 2010. Application of oxygen eddy
580   correlation in aquatic systems. Journal of Atmospheric and Oceanic Technology **27:** 1533-1546.

MacIntyre, S., A. Jonsson, M. Jansson, J. Aberg, D. E. Turney, and S. D. Miller. 2010. Buoyancy flux, turbulence, and the gas transfer coefficient in a stratified lake. Geophysical Research Letters **37**.

Macintyre, S., R. Wanninkhof, and J. P. Chanton. 1995. Trace gas exchange across the air-water interface in freshwater and coastal marine environments, p. 52-97. *In* R. C. H. P.A. Matson [ed.],
585   Biogenic Trace Gases: Measuring Emissions from Soil and Water. Blackwell Science Ltd.

Mammarella, I., A. Nordbo, Ü. Rannik, S. Haapanala, J. Levula, H. Laakso, A. Ojala, O. Peltola, J. Heiskanen, J. Pumpanen, and T. Vesala. 2015. Carbon dioxide and energy fluxes over a small boreal lake in Southern Finland. Journal of Geophysical Research: Biogeosciences**:** 2014JG002873.

590   Marino, R., and R. W. Howarth. 1993. Atmospheric oxygen-exchange in the Hudson River - Dome measurements and comparison with other natural-waters. Estuaries **16:** 433-445.

McKenna, S., and W. McGillis. 2004. The role of free-surface turbulence and surfactants in air–water gas transfer. International Journal of Heat and Mass Transfer **47:** 539-553.

Odum, H. T. 1956. Primary production in flowing waters. Limnol. Oceanogr. **1:** 103-117.

595   Raymond, P., and J. Cole. 2001. Gas exchange in rivers and estuaries: Choosing a gas transfer velocity. Estuaries **24:** 312-317.

Raymond, P. A., J. Hartmann, R. Lauerwald, S. Sobek, C. McDonald, M. Hoover, D. Butman, R. Striegl, E. Mayorga, C. Humborg, P. Kortelainen, H. Durr, M. Meybeck, P. Ciais, and P. Guth. 2013. Global carbon dioxide emissions from inland waters. Nature **503:** 355-359.

600   Raymond, P. A., C. J. Zappa, D. Butman, T. L. Bott, J. Potter, P. Mulholland, A. E. Laursen, W. H. McDowell, and N. D. 2012. Scaling the gas transfer velocity and hydraulic geometry in streams and small rivers. Limnology and Oceanography: Fluids & Environments **2:** 41-53.

Rheuban, J. E., P. Berg, and K. J. McGlathery. 2014. Multiple timescale processes drive ecosystem metabolism in eelgrass (*Zostera marina*) meadows. Marine Ecology Progress Series **507:** 1–13.

605   Rovelli, L., K. M. Attard, L. D. Bryant, S. Flögel, H. J. Stahl, M. Roberts, P. Linke, and R. N. Glud. 2015. Benthic O2 uptake of two cold-water coral communities estimated with the non-invasive eddy-correlation technique. Marine Ecology Progress Series **525:** 97-104.

Van de Bogert, M. C., D. L. Bade, S. R. Carpenter, J. J. Cole, M. L. Pace, P. C. Hanson, and O. C. Langman. 2012. Spatial heterogeneity affects estimates of ecosystem metabolism in two

610   northern lakes. Limnol. Oceanogr. **57:** 1689-1700.

Van de Bogert, M. C., S. R. Carpenter, J. J. Cole, and M. L. Pace. 2007. Assessing pelagic and benthic metabolism using free water measurements. Limnology And Oceanography-Methods **5:** 145-155.

Wanninkhof, R. 1985. Kinetic fractionation of the carbon isotopes 13C and 12C during transfer of CO2

615   from air to seawater. Tellus B **37:** 128-135.

Wanninkhof, R., P. J. Mulholland, and J. W. Elwood. 1990. Gas-exchange rates for a 1st-order stream determined with deliberate and natural tracers. Water Resources Research **26:** 1621-1630.

Watson, A. J., R. C. Upstill-Goddard, and P. S. Liss. 1991. Air–sea gas exchange in rough and stormy seas measured by a dual-tracer technique. Nature **349:** 145-147.

620   Whitman, W. G. 1923. The two film theory of gas absorption. Chemical and Metallurgical Engineering **29:** 146-148.

9 Tables

Deployment	Start date	n	Current velocity	O_2 flux	k_{600}
-	-	-	cm s^{-1}	mmol m^{-2} d^{-1}	m d^{-1}
Hardware River, dep. 1	Nov 22, 2015	20	28.4	9.1	1.6
"	"	39	27.5	12.0	2.7
"	"	13	27.6	-10.7	2.5
Hardware River, dep. 2	Sep 14, 2016	20	8.7	7.0	0.4
"	"	4	8.3	9.4	0.7
Mechums River	Dec 21, 2016	23	9.4	-42.9	2.3
"	"	36	9.3	-29.2	1.7
Moormans River	Jan 18, 2017	4	25.6	-8.9	1.9
"	"	51	18.4	16.8	3.9
"	"	34	20.4	-11.8	1.3
"	"	3	22.9	19.3	5.1
"	"	16	23.4	10.1	2.1
"	"	26	21.3	5.8	1.0

Table 1: Representative standard gas exchange coefficients (k_{600}) along with current velocity and O_2 flux for four deployments at three different sites. The third column (n) specifies the number of 15-min time intervals included in the averages. Values from the last deployment (Moormans River) are depicted in Figs. 2 and 3.

10 Figures

Figure 1: Floating platform for determining air-water gas exchange. **(a)** The 1.2 × 0.9 m wide platform with a catamaran-shaped hull being prepared for deployment. Four inflatable fenders provide flotation. **(b)** The platform deployed in the Hardware River and anchored to both river banks. A dive weight is used to level the platform. **(c)** Close-up look at: 1) the three-pronged upward-facing sensor head of the cabled Acoustic Doppler Velocimeter (cabled Vector, Nortek AS, Norway), 2) the fast-responding dual O_2-temperature sensor (RINKO EC, JFE Advantech, Japan), and 3) Two stable independent dual O_2-temperature sensors used for calibration (miniDOT, PME, USA).
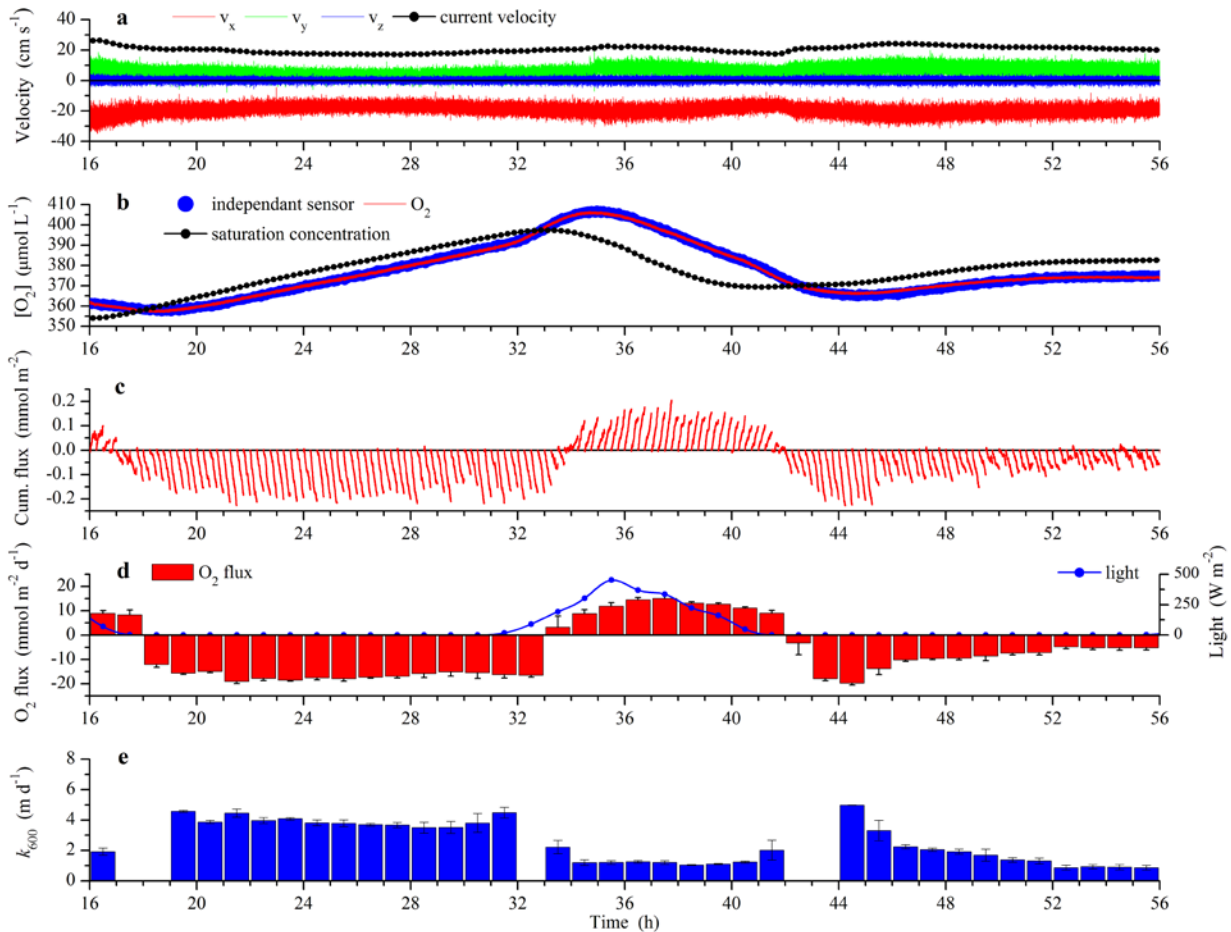
Figure 2: Forty h long test deployment initiated at 16:00 in the afternoon as indicated on the x-axis. **(a)** Three velocity components at 8 Hz (x, y, z; z is vertical) and 15-min mean current velocity. **(b)** O_2 concentration at 8 Hz measured with the dual O_2-temperature sensor and at 1-min measured with an independent sensor. **(c)** Cumulative flux over 15-min time intervals with clear linear trends. **(d)** Hourly O_2 flux (positive values represent a release from the river), each value based on 15-min flux extractions (n = 4, SE) and day light measured at a nearby weather station. **(e)** Hourly standard gas exchange coefficient (k_{600}) based on 15-min estimates (n = 4, SE). The few gaps in the data are for the times where the driving O_2 concentration difference changes sign (panel **c**).
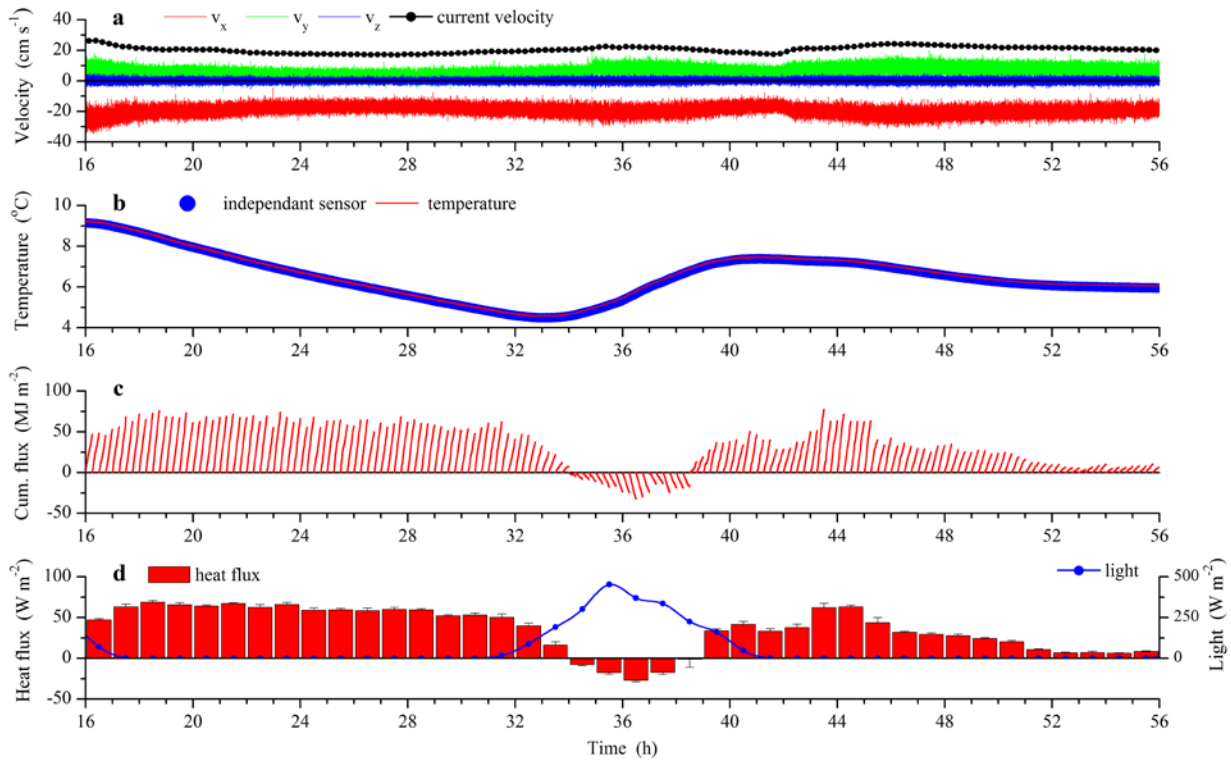
Figure 3: The same deployment as in Fig. 2, but with results for temperature and heat. The deployment was initiated at 16:00 in the afternoon as indicated on the x-axis. **(a)** Three velocity components at 8 Hz (x, y, z; z is vertical) and 15-min mean current velocity. **(b)** Temperature at 8 Hz measured with the dual O_2-temperature sensor and at 1-min measured with an independent optode. **(c)** Cumulative flux over 15-min time intervals with clear linear trends. **(d)** Hourly heat flux, each value based on 15-min flux extractions (n = 4, SE) and day light measured at a nearby weather station. Positive flux values represent a release of heat from the river.
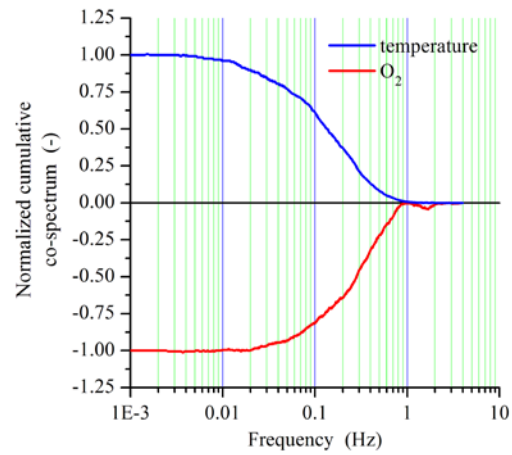
Figure 4: Nighttime normalized cumulative co-spectra for the vertical velocity combined with the O_2 concentration and the temperature, respectively, revealing which frequencies carried the eddy flux signal.
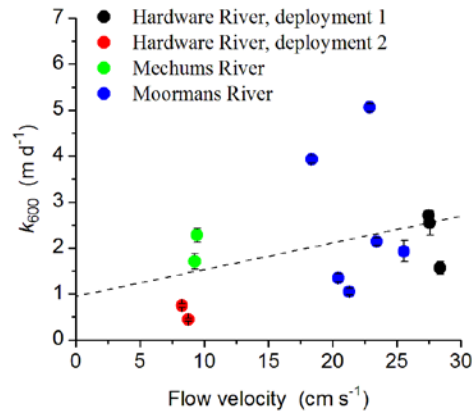
Figure 5: Standard gas exchange coefficient, k_{600}, plotted against river current velocity. The dotted line is a linear fit to all data (R = 0.37, p = 0.22).
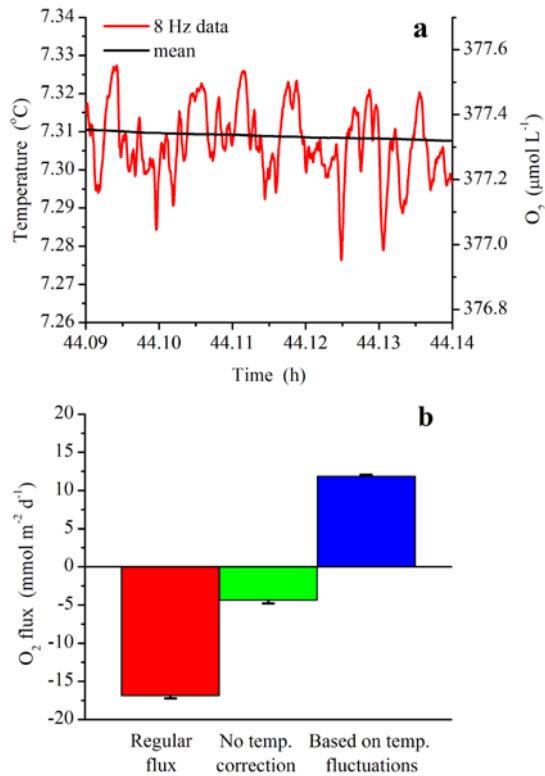
Figure 6: Bias that can arise if O_2 concentration sensor readings are not corrected using rapid parallel temperature measurements. **(a)** Recorded 8 Hz data of temperature fluctuations and their mean (left axis) through 3-min and the resulting fluctuations in O_2 concentration that would be recorded solely due to temperature sensitivity by a sensor with a temperature coefficient of 3 % (right axis). **(b)** Average air-water fluxes, all for the same period of the first night (h 18 to h 32) of the deployment depicted in Figs. 2 and 3, calculated using instantaneous temperature corrected data (red bar), data without temperature correction (green bar), and 'simulated' data produced from 8Hz temperature recordings as shown in panel **a** and assuming a temperature coefficient of 3 % (blue bar).